

Validation of Registration for Renal Dynamic Contrast Enhanced MRI Imaging

Seniha Esen Yuksel *¹

Accepted 10th August 2016

DOI: 10.18201/ijisae.45496

Abstract: In Dynamic Contrast Enhanced Resonance Imaging (DCE-MRI), abdomen is scanned repeatedly and rapidly after injection of a contrast agent. During data acquisition, collected images suffer from the motion induced by the patient if he/she moves or breathes heavily during the scan. Therefore, these images should be aligned accurately to correct the motion. Recently, mutual information (MI) registration has become the first tool to register renal DCE-MRI images before any further processing. However, MI registration is sensitive to initial conditions and optimization methods, and it is bound to fail under certain conditions such as extreme movement or noise in the image. Therefore, if automated image analysis for renal DCE-MRI is to enter the clinical settings, it is necessary to have validation strategies that show the limitations of registration models on known datasets. In this study, two methods are introduced for the validation of registration of renal DCE-MRI images. The first method demonstrates how to use the inverse transform to generate realistic looking DCE-MRI kidney images and use them in validation. The second method shows how to generate checkerboard images and how to evaluate the goodness of registration for real DCE-MRI images. These validation methods can be incorporated into the registration studies to quantitatively and qualitatively demonstrate the success and the limitations of registration models.

Keywords: Contrast-enhanced magnetic resonance imaging, inverse transform, mutual information, registration, validation.

1. Introduction

Dynamic Contrast Enhanced Resonance Imaging (DCE-MRI) is an imaging technique in which the abdomen is scanned repeatedly and rapidly after the injection of a contrast agent. As the contrast agent perfuse into the kidney, it creates an intensity change in the images as shown in Fig. 1. The pattern of this intensity change is an indicator of the kidney's functionality and it can be used in determining the type of kidney dysfunction. For example, if the intensity change is not reaching to high levels in a short amount of time, the kidney might not be filtering properly and the patient might need drug therapies [1,2]. Therefore, DCE-MRI has become a very valuable tool in renal disease diagnosis as it is safe, sensitive, non-invasive and provides not only anatomical but also functional information. Furthermore, each functional renal compartment (renal cortex, medulla and the collecting system) can be independently evaluated and kidney glomerular filtration rate can be computed from a single kidney. As a result, there has been valuable amount of recent re- search in the image analysis of kidney DCE-MRI data to assess renal blood flow, understand kidney function, and evaluate several clinical disorders [3–23].

In DCE-MRI of kidneys, the intensity change plotted over time is called a renogram [13]. A typical image analysis procedure to arrive at the renogram curves requires five major steps: (1) globally aligning the sequence of images (rigid registration), (2) segmenting the kidney into cortex and medulla structures, (3) realigning the sequence of images if non-rigid movements are

present, (4) extracting and plotting the renograms from the cortex and medulla, and (5) classifying these renograms. The first step, registration, refers to spatially aligning the images and cancelling out any movement of the abdomen over time, as illustrated in Fig. 2. Clearly, the success of this step affects the success of all the following image analysis steps, and any error in registration is propagated all the way to classification. Several studies have addressed the registration problem and many used mutual information (MI) registration as the first step [3–6, 12–15, 24–40].

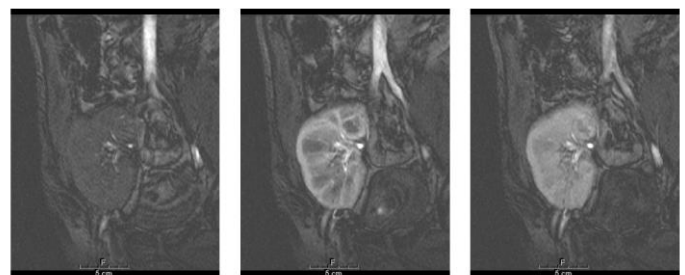


Figure 1: Example of a DCE-MRI series. For each patient, 150 images are taken from one cross section with 4 second intervals. Shown here are three images demonstrating the uptake of the contrast agent. The change in the signal intensity follows different patterns for the cortex and medulla structures.

¹ Hacettepe University, Department of Electrical and Electronics Engineering, Ankara, Turkey.

* Corresponding Author: Email: eyuksel@ee.hacettepe.edu.tr

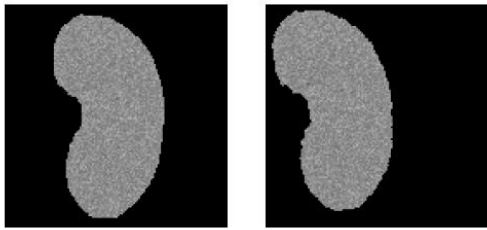


Figure 2: Illustration of the misalignment of two images. In these images, compared with one another, the anatomical structure is located at different positions. A rigid registration would translate and rotate the right image to align it with the left image.

These registration studies are aimed towards solving multiple complexities that arise during renal image alignment in DCE-MRI. Some of these challenges can be listed as: (1) the lack of fiducial markers on the kidneys, (2) the change in the intensity in a DCE-MRI image during data acquisition, (3) the variability in motion in real datasets both before and during the data acquisition and (4) the lack of standardized image acquisition protocols and a lack of a standard dataset. These challenges make it very hard to prove the accuracy of the registration methods, and require carefully studied validation strategies.

Validation refers to quantitatively and qualitatively evaluating the quality of the transformation models, reporting the accuracy of the computed models as well as determining the limits of registration and finding the bounds on error, i.e. reporting when a model works best and under which conditions it would fail. The need for validation strategies was discussed in the editorial paper by Jannin et al. [41] for all medical studies, which pointed to a neglect in validation studies, saying "... validation is usually addressed only as a section in the paper. However, validation is by itself a research topic where methodological innovation and research are required". Unfortunately, DCE-MRI studies have been suffering from the same problem, and many of the above studies lack the necessary validation strategies that are needed prior to clinical use.

In this study, two validation methods are proposed that can be incorporated into the DCE-MRI registration studies to test the accuracy of these registration methods: (1) inverse transform and (2) checkerboard validation with edge-based quantitative measures. The first method, inverse transform, is used to create realistic synthetic images from the original dataset. Such a synthetic dataset is useful to demonstrate the capabilities of the registration algorithms and to get a quantitative analysis of the conditions under which the registration algorithms would no longer be acceptable. The second method, checkerboard validation, is used to check the accuracy of the registration methods on the real data quantitatively and qualitatively. Both inverse transform and checkerboard validation methods are independent of the image acquisition protocol and can be applied to a wide range of rigid registration algorithms.

For DCE-MRI, mutual information (MI) registration [42] has been used as the first step of the 5-step image analysis framework in several studies including [3–6, 12–15, 24–26]; or has been the baseline for other algorithms such as [27]. MI has been chosen as the metric of registration in these studies mostly because it is very effective in multi-modal image registration and the intensity change in DCE-MRI images can be regarded as a multi-modality. Therefore, in the rest of this paper, MI registration is taken as a baseline and validation strategies are described on the MI registration of DCE-MRI images.

First, data acquisition protocol is given in Sec. 2 and MI registration is described in Sec. 3. Then, Sec. 4 introduces the

inverse transform, demonstrates how to generate realistic looking synthetic images, discusses how to analyze the results and finds where the registration methods are no longer applicable or dependable. Finally, checkerboard-imaging validation is presented in Sec. 5 and the results are shown on real DCE-MRI data.

1. Data Acquisition

Gradient echo T1 imaging is employed by a Signa Horizon GE 1.5T scanner (Signa Horizon LX Echo speed; General Electric Medical Systems, Milwaukee, WI, USA) with the use of phased array Torso surface coil, and the contrast agent Gadolinium diethylene triamine pentaacetic acid (Gd-DTPA) is introduced via a wide bore veno-catheter placed at antecubital vein at a rate of 3–4 ml/sec with a dose of 0.2 ml/kg.BW. Images are taken at 5mm thickness with no inter-slice gap, repetition time (TR) 34 msec, TE minimum, field of view (FOV) 42×42 cm and matrix of 1005×804 . For each patient, 150 temporal sequences of coronal scans are taken with 4 second intervals.

2. Mutual Information Registration

In DCE-MRI, the abdomen is scanned repeatedly after the administration of the contrast agent. During the scanning process, the patient may breathe or move unintentionally, so the position of the kidney can change from one scan to another. To perform an accurate slice-by-slice comparison of these images, kidney images should first be aligned to each other. The alignment of two images is called registration, and if only translational and rotational movements are considered, the alignment process is called rigid registration. One of the rigid registration methods, mutual information (MI) registration, has been proven to align images from different modalities (such as MRI and CT) accurately and robustly [42–46]. Similarly, it has been successful in handling the contrast change in renal DCE-MRI images without requiring any fiducial markers, landmarks or feature extraction.

Let A and B be two images that are to be registered. Let a and b be the gray values of images A and B with marginal densities $p_A(a)$ and $p_B(b)$. These marginal densities correspond to the normalized histograms. Also, define $p_{AB}(a,b)$ as the joint distribution of the images' gray values, which corresponds to the joint histogram. Normalized mutual information [47] measures the amount of information that one image A contains about the other image B as:

$$NMI(A, B) = \frac{H(A) + H(B)}{H(A, B)} \quad (1)$$

where $H(A)$ and $H(B)$ are the marginal entropies of images A and B respectively, and $H(A, B)$ is the joint entropy of these images. These entropies are computed from the probability density functions of the images' gray values as:

$$\begin{aligned}
H(A) &= - \sum_{a \in A} p_A(a) \log p_A(a) \\
H(B) &= - \sum_{b \in B} p_B(b) \log p_B(b) \\
H(A, B) &= - \sum_{a \in A} \sum_{b \in B} p_{AB}(a, b) \log p_{AB}(a, b)
\end{aligned} \tag{2}$$

Mutual information measures the dependence of the two images. MI is maximized when there is a maximal dependence between the gray values of the images, and this happens when the images are correctly aligned [42]. The more similar (i.e. the less independent) the images are, the lower the joint entropy compared to the sum of the individual entropies i.e. $H(A; B) \leq H(A) + H(B)$. Therefore, two images are best aligned by a transformation function T when $H(A; B)$ is minimized and $NMI(A; B)$ in Eq. (1) is maximized. To calculate Eq. 1, one has to compute the joint densities in Eq. 2. One way to compute these joint densities is by Parzen windowing. In Parzen windowing, an intensity sample S of size N_s is drawn from the image. Then, the probability $p_A(a)$ is computed as the sum of the contributions of each sample from S to $p_A(a)$ in accordance with its distance from a . The Parzen estimate can be obtained from the following equation:

$$p_A(a) = \frac{1}{N_s} \sum_{s_j \in S} K(a - s_j) \tag{3}$$

where s_j is the intensity (gray level) of the j^{th} pixel in the sample set S , and K is generally a Gaussian kernel in the form of $K(u) = \exp(-u^2/2\sigma^2)$ with variance σ^2 . To calculate the entropy, another intensity sample R of size N_r is drawn from the image, and the entropy is calculated with the following equation:

$$H(A) = \frac{1}{N_r} \sum_{r_j \in R} \log p(r_j) \tag{4}$$

where r_j is the intensity of the j^{th} pixel in the sample set R . Parzen windowing gives a smooth solution to density estimation. However, if the variance σ^2 is selected to be too large, then important modes in the density may be filtered out during smoothing. Likewise, a small variance value results in a noisy density estimate.

In the implementation of mutual information, relatively high noise in the images can sometimes be a problem. With increased noise, the entropy can be determined by the noise instead of the original signal, affecting the performance of the registration. To minimize such problems, the kidneys are cropped from the rest of the abdomen before the registration, resulting in a smaller region of interest which includes mostly the kidneys.

The code was written into C++ with the use of ITK libraries [48]. Images were smoothed with Gaussian kernels with a variance of 2.0. For the gradient descent optimization the step size (learning rate) was chosen to be 0.02 and the maximum number of iterations were set to 500. Another important parameter is the number of randomly selected samples from an image for the Parzen windowing. If the sample size is selected to be large, the metric is smoother from one iteration to another, but at the expense of longer computation times. In our implementation, we found $N_s = 500$ and $\sigma = 0.4$ to be reasonable approximations. These parameters are listed in Table 1.

TABLE 1: Mutual Information Registration Parameters

Fixed Image & Moving Image	Standard Deviation	0.4
	Smoothing Variance	2.0
Number of Spatial Samples		500
Learning Rate		0.02
Number of Iterations		500

3. Validation of Registration Using Synthetic Images: Inverse Transform Sampling

One way to validate registration results is by generating realistic looking phantom images, transforming them with known parameters, and applying the registration techniques to revert them back to the initial conditions. This technique gives the limit of transformation to be able to successfully register the images and shows how much of the transformation is recoverable. In addition, it allows to test the effect of image noise on registration models. Such noise analysis is especially important in DCE-MRI as increasing the speed of image acquisition results in a better temporal resolution at the expense of noisier images.

In this study, kidney phantoms were generated with known translation and rotation parameters to validate the registration results on renal DCE-MRI. Kidney phantoms are realistic looking synthetic images that have the medulla and cortex structures as shown in Fig. 3(j,k,l). These images were generated using inverse transform sampling (ITS). ITS [49] is a method for pseudo-random number sampling which generates samples from a probability distribution with a known cumulative distribution function (CDF). In order to use ITS, first, densities (normalized histograms) were obtained from the cortex and medulla compartments of real DCE-MRI images of kidneys. Second, CDFs were obtained from these structures as well as the background. Then, ITS was used to generate random variables with similar distributions. These random variables become the gray level values in the phantoms where the gray levels of background, cortex and medulla structures resemble the noise and intensity levels of the original images.

Let X be a random variable whose distribution can be described by the CDF F . To generate a continuous random variable X that is distributed according to this distribution such that $X \sim F$, the ITS works as follows:

- 1) Generate a uniform random variable U from the standard uniform distribution in the interval $[0,1]$.
- 2) Compute the value X such that $X = F^{-1}(U)$.
- 3) Take X to be the random number drawn from the distribution described by F .

To apply the inverse transform for a discrete random variable $X = \{X_1, X_2, \dots, X_n\}$, the second step is modified as: $\{X = x_j \text{ if } F_X(x_{j-1}) \leq U < F_X(x_j)\}$. The pseudo-code for ITS for the discrete case is as follows:

Algorithm 4.1: INVERSE TRANSFORM (A)

```

Obtain  $F$  from the object of interest in image  $A$ 
for each pixel ( $k1, k2$ ) in the region of interest of the mask image
    Get  $U = \text{rand}()$ 
do
    find number of pixels  $N_p$  such that  $F \leq U$ 
    Output Image( $k1; k2$ ) =  $N_p$ 
return (Output Image)

```

ITS is demonstrated in Fig. 3 in three steps. In the first step, three images with well identifiable cortex and medulla structures were chosen from one patient as shown in Fig. 3(a-c). These indicate the first image of the sequence, an early enhancement image and a late enhancement image. From these images, Fig. 3(b) was used as to create a mask, and the gray level values of this mask were assigned using inverse transform.

In the second step, normalized histograms of these three images were calculated as shown in Fig. 3(d-f) for the cortex, the medulla and the background. Then, cumulative distribution functions were obtained as displayed in Fig. 3(g-i). In the third step, these CDF's were used in ITS to generate realistic phantoms. To obtain the gray values of the phantoms, for each pixel in the mask, a random variable was generated with ITS, and this random variable was used as the gray level of the phantom image as given in the pseudocode 4.1. An example of the phantom images for zero rotations and translation is given in Fig. 3(j-l).

Finally, the mask image was transformed with several rotations and translations as shown in Fig. 4(a-c). After the transformations, these masks were assigned their gray values with ITS as described above. The phantoms generated for Fig. 3(b) are shown in Fig. 6(a-c) for three different transformations. Let these images be denoted as test sequence 1. Similarly, the phantoms generated for Fig. 3(a) are given in Fig. 5(a-c), and are referred to as the test sequence 2. All of these test images in Fig. 6 and Fig. 5 were registered to Fig. 3(l). The original rotation and translation values and the estimated results using mutual information registration are given at Tables 2 and 3 for the test sequences 1 and 2, respectively. The first three columns of these tables show the original transformations, the next three columns are the results obtained by mutual information registration, and the last column is the normalized MI metric (i.e. the similarity measure of the registration). In the tables, we refer to Fig. 3(l) as the reference image.

TABLE 2: Registration of test sequence 1 to the reference image: robustness to translation (in pixels) and rotation (in degrees). Rotation is denoted by R, translation in X is denoted by T_X and the translation in the Y direction is denoted by T_Y .

Original			Estimated			Metric Value
R	T_X	T_Y	Rotation	Translation X	Translation Y	
0	0	0	-0.14	0.30	0.58	0.45
0	5	0	0.24	5.60	0.10	0.44
0	0	5	0.06	-0.53	5.26	0.44
5	0	0	5.46	-0.70	-0.24	0.44
5	5	0	5.10	4.70	0.31	0.43
5	0	5	5.10	4.70	0.31	0.43
5	5	5	5.16	5.08	5.08	0.44
10	0	0	9.85	-0.51	-0.06	0.44
0	10	10	0.18	9.79	9.76	0.44
10	5	5	10.23	5.11	5.35	0.39
10	10	10	10.04	8.01	11.65	0.44
0	20	20	-0.14	20.17	20.05	0.44
10	20	20	10.11	16.62	22.80	0.43

TABLE 3: Registration of test sequence 2 to the reference image: robustness to translation (in pixels) and rotation (in degrees). Rotation is denoted by R, translation in X is denoted by T_X and the translation in the Y direction is denoted by T_Y .

Original			Estimated			Metric Value
R	T_X	T_Y	Rotation	Translation X	Translation Y	
0	0	0	0.34	-0.35	-1.94	0.026
0	5	0	-1.86	5.54	0.37	0.027
0	0	5	1.34	-1.66	3.82	0.019
5	0	0	2.03	0.02	0.46	0.023
5	5	0	3.24	5.79	1.25	0.029
5	5	5	6.15	6.71	6.31	0.029
10	0	0	6.36	2.02	-0.88	0.029
0	10	10	1.31	8.28	6.02	0.022
10	5	5	6.77	3.57	3.84	0.029
10	10	10	9.82	11.23	9.61	0.028

In Table 2, mutual information registration is able to handle the transformations with subpixel accuracy for small translations under five pixels and rotations under five degrees. For bigger transformations, it deviates with a couple of pixels until reaching a breaking point at the end of the table for 10 degrees of rotation and 20 pixels of translation in each axis. Note that 4 pixels correspond to 17mm in the x-axis and 20mm in the y-axis as explained in Sec. 2. Some of this error in accuracy can easily be handled by decreasing the learning rate of the optimizer and by increasing the number of iterations. However, when the boundaries are harder as in the test sequence 2, the MI metric values are much smaller. In Table 3, the results are still acceptable for small translations and rotations, but the MI metric starts to decrease in accuracy with higher translations and rotations. Therefore, it is very important to know the maximum translation and rotation values one would expect in a typical clinical setting and compare that to these values. Moreover, it is also important to at least visually confirm that registration gives meaningful results. In the next section, a second method is presented to qualitatively and quantitatively confirm the goodness of registration on kidney DCE-MRI images.

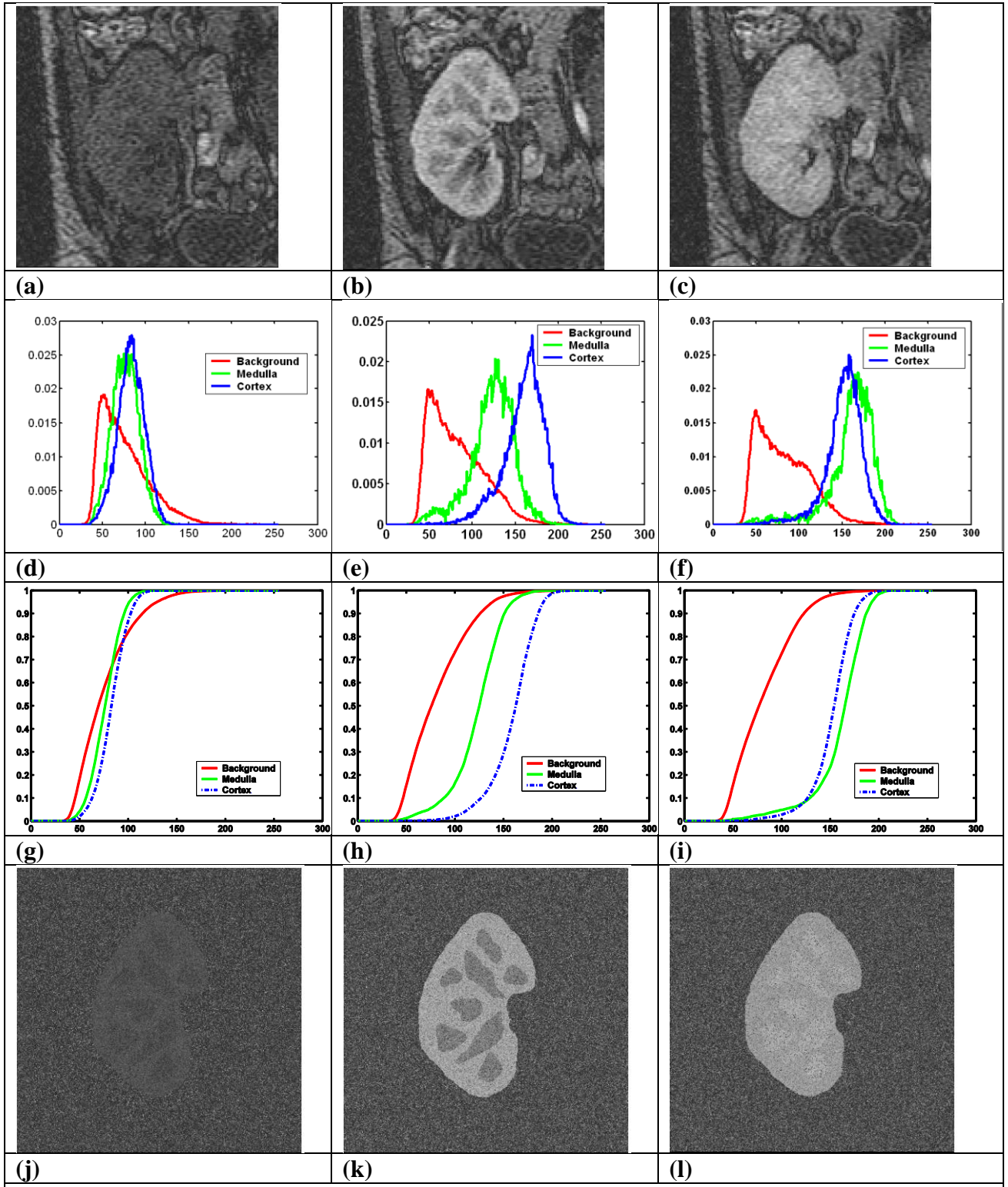


Figure 3: Three images from a sequence (a,b,c), their gray level densities (d,e,f) and the cumulative distributions (CDF's) (g, h, i). A mask is obtained from (b), and by inverse transform, the test images (j, k, l) are obtained for zero translation and rotation.

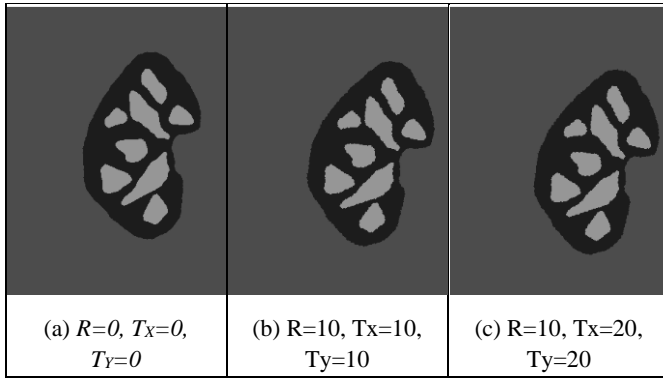


Figure 4: A mask image is generated manually based on the real kidney image in Fig. 3(b). This mask is transformed with various rotations (R in degrees) and translations in x direction (T_x) and in y direction (T_y) in pixels. Three of them are shown here.

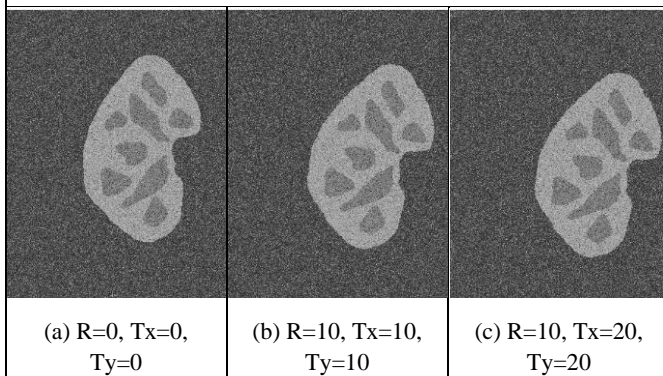


Figure 5: Test Sequence 1. Background, cortex and medulla structures in the mask are filled separately with random variables obtained via inverse transform from the gray level CDF's (Fig. 3(h) of Fig. 3(b)).

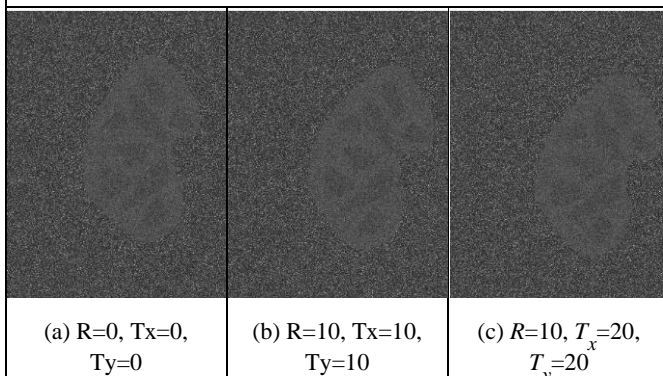


Figure 6: Test Sequence 2. Background, cortex and medulla structures in the mask are filled separately with random variables obtained via inverse transform from the gray level CDF's (Fig. 3(g) of Fig. 3(a)).

4. Validation of Registration: Checkerboard Imaging

A checkerboard image is obtained by patching one square region from the fixed image and another square region from the moving image after registration, and these patches are visualized in one checkerboard image. In a checkerboard image, the expectation is to see continuous contours. If two images are correctly registered, the contours of the kidneys and other structures should be aligned, and should show continuously lines as opposed to having discrete disparities. Disparities between these two images indicate errors, which may be due to the problems with the transformation model itself, or the inaccuracies in the parameters.

With the observation that mutual information registration gives satisfactory results on phantom images, the registration technique has been applied to real abdomen images. The cropped time series of a patient were aligned using mutual information registration to cancel the breathing and movement errors. The resulting images were visually tested by checkerboards. Between each square, continuous contours were well obtained in the resulting checkerboard images as shown in Figs. 7 and 8.

Although checkerboard imaging is a qualitative way to validate registration, it can also be extended for quantitative use. One option would be to compute the edges and do a connected component analysis to see if they are continuous. Another option would be to compute the mutual information within each square and expect a smooth MI metric over all the squares. This option also brings the following advantage: if most of the squares have similar MI metrics but one of the neighbouring square is much lower or higher than the others, this could indicate the existence of a non-rigid transformation.

5. Conclusion

DCE-MRI is a noninvasive test that provides high spatial and temporal resolution of a single kidney, and allows evaluating the state of the cortex and medulla structures separately. In the recent years, many studies have focused on automatic image analysis of the DCE-MRI images to differentiate between several kidney diseases. Registration is one of the key components in these image analysis techniques, and the quality of registration models need to be validated before automated analysis of DCE-MRI can enter the clinical settings. In this study, two validation techniques were introduced for the validation of registration in renal DCE-MRI images: inverse transform sampling and checkerboard imaging. With inverse transform sampling, a way to generate synthetic kidney images that follow the noise structure of real DCE-MRI images was demonstrated. Then how to test the goodness of registration was shown with these images under various translations and rotations. In these tests, mutual information was used as the method of registration. Qualitative metric values were obtained, bounds on error were obtained and the limits on registration for this data collection were reported. In the second validation method, the cropped time series of a patient were aligned using mutual information registration to cancel the breathing and movement errors. Then the registered images were displayed as checkerboard images. The existence of continuous contours in checkerboard images provides a qualitative validation on the goodness of registration.

With these two fold validation techniques, a robust and flexible system has been presented that can be used to address a variety of image registration problems. The validation framework presented in this paper presents a generic approach to both simulate kidney images as well as work on real kidney images. These validation strategies could be used to help improve any rigid registration algorithm, to compare the registration performance of a set of rigid registration methods, as well as to evaluate the goodness of registration in a clinical environment.

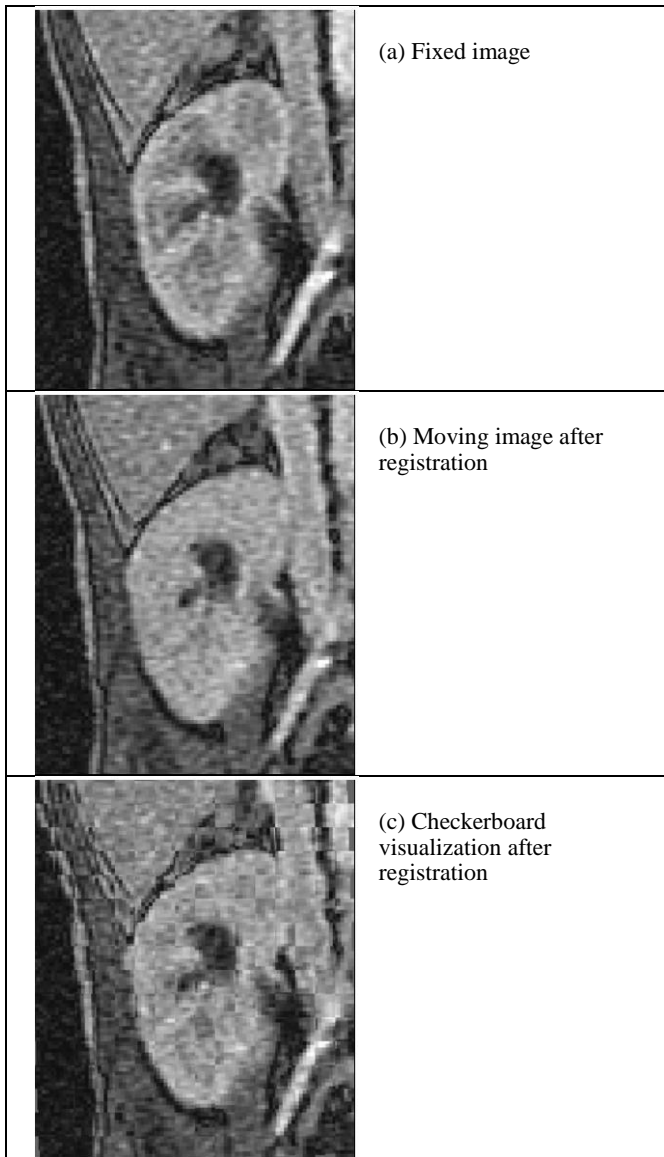


Figure 7: Sample registration results for two images from one data set. The moving image in (b) is registered to the fixed image in (a), and the resultant registration is shown in (c). A checkerboard image is generated from (a) and (c) to test the quality of the registration visually. Registration results: Rotation $R=1.82$ degrees, translation in x direction $T_x=1.49$ pixels, translation in y direction $T_y=0.78$ pixels, MI metric = 0.27129.

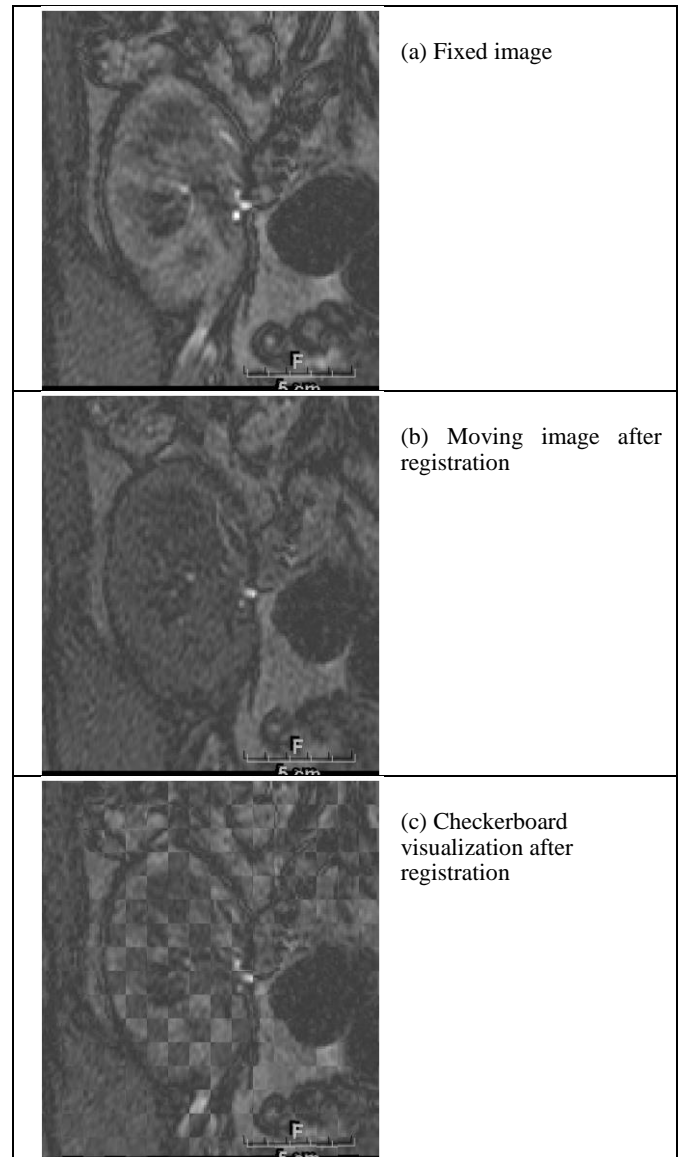


Figure 8: Sample registration results for two images from one data set. The moving image in (b) is registered to the fixed image in (a), and the resultant registration is shown in (c). A checkerboard image is generated from (a) and (c) to test the quality of the registration visually. Registration results: Rotation $R=0.478$ degrees, translation in x direction $T_x= 2.34$ pixels, translation in y direction $T_y= -0.11$ pixels, MI metric = 0.183.

References

- [1] M. Notohamiprodjo, M. F. Reiser, S. P. Sourbron, Diffusion and perfusion of the kidney, *European Journal of Radiology* 76 (3) (2010) 337 – 347.
- [2] G. Brix, S. Zwick, J. Griebel, C. Fink, F. Kiessling, Estimation of tissue perfusion by dynamic contrast-enhanced imaging: simulation-based evaluation of the steepest slope method, *European Radiology* 20 (9) (2010) 2166–2175.
- [3] V. Positano, I. Bernardeschi, V. Zampa, M. Marinelli, L. Landini, M. Santarelli, Automatic 2D registration of renal perfusion image sequences by mutual information and adaptive prediction, *Magnetic Resonance Materials in Physics, Biology and Medicine* 26 (3) (2013) 325–335.
- [4] F. Khalifa, G. Beache, T. El-Diasty, G. Gimelfarb, M. Kong, A. El-Baz, Dynamic contrast-enhanced MRI-based early detection of acute renal transplant rejection, *IEEE transactions on medical imaging* 32 (10) (2013), 1910–1927.
- [5] F. Khalifa, M. Abou El-Ghar, B. Abdollahi, H. B. Frieboes, T. El-Diasty, A. El-Baz, A comprehensive noninvasive framework for automated evaluation of acute renal transplant rejection using DCE-MRI, *NMR in Biomedicine* 26(11) (2013).
- [6] F. Zollner, R. Sance, P. Rogelj, M. J. Ledesma-Carbayo, J. Rorvik, A. Santos, A. Lundervold, Assessment of 3D DCE-MRI of the kidneys using non-rigid image registration and segmentation of voxel time courses., *Comp. Med. Imag. and Graph.* 33 (3) (2009) 171–181.
- [7] X. Li, X. Chen, J. Yao, X. Zhang, F. Yang, J. Tian, Automatic renal cortex segmentation using implicit shape registration and novel multiple surfaces graph search,

- Medical Imaging, IEEE Transactions on 31 (10) (2012) 1849–1860.
- [8] O. Gloger, K. Tonnie, V. Liebscher, B. Kugelmann, R. Laqua, H. Volzke, Prior shape level set segmentation on multistep generated probability maps of MR datasets for fully automatic kidney parenchyma volumetry, *Medical Imaging, IEEE Transactions on* 31 (2) (2012) 312–325.
- [9] P. Gujral, M. Amrhein, D. Bonvin, J.P. Vallee, X. Montet, N. Michoux, Classification of magnetic resonance images from rabbit renal perfusion, *Chemometrics and Intelligent Laboratory Systems* 98 (2) (2009) 173 – 181.
- [10] G. Chiusano, A. Stagliano, C. Basso, A. Verri, DCE-MRI Analysis Using Sparse Adaptive Representations, Vol. 7009, *Machine Learning in Medical Imaging, Lecture Notes in Computer Science*, Springer, 2011, pp. 67–74.
- [11] L. Ruthotto, E. Hodneland, J. Modersitzki, Registration of dynamic contrast enhanced MRI with local rigidity constraint, in: *Proceedings of the 5th international conference on Biomedical Image Registration*, Springer-Verlag, 2012, pp. 190–198.
- [12] S. E. Yuksel, A. El-Baz, A. A. Farag, M. El-Ghar, T. Eldiasty, M. A. Ghoneim, A kidney segmentation framework for dynamic contrast enhanced magnetic resonance imaging, *Journal of Vibration and Control* 13 (9-10) (2007) 1505–1516.
- [13] S. E. Yuksel, A. El-Baz, A. A. Farag, M. El-Ghar, T. Eldiasty, M. A. Ghoneim, Automatic detection of renal rejection after kidney transplantation, in: *Proc. of Computer Assisted Radiology and Surgery (CARS)*, 2005, pp. 773–778.
- [14] A. A. Farag, A. El-Baz, S. E. Yuksel, M. El-Ghar, T. Eldiasty, A framework for the detection of acute renal rejection with dynamic contrast enhanced magnetic resonance imaging, in: *Proceedings of International Symposium on Biomedical Imaging (ISBI)*, 2006, pp. 418–421.
- [15] A. El-Baz, R. Fahmi, S. E. Yuksel, A. A. Farag, W. Miller, M. El-Ghar, T. Eldiasty, A new CAD system for the evaluation of kidney diseases using DCE–MRI, in: *Proc. of International Conference on Medical Image Computing and Computer Assisted Intervention (MICCAI)*, Vol. 2, 2006, pp. 446–453.
- [16] B. Chevaillier, J.L. Collette, D. Mandry, M. Claudon, O. Pietquin, Objective assessment of renal DCE-MRI image segmentation, in: *Proceedings of the European Signal Processing Conference (EUSIPCO)*, 2010, pp. 1214–1218.
- [17] L. Bokacheva, H. Rusinek, J. L. Zhang, V. S. Lee, Assessment of renal function with dynamic contrast-enhanced MR imaging, *Magnetic Resonance Imaging Clinics of North America* 16 (4) (2008) 597 – 611.
- [18] B. Chevaillier, Y. Ponvianne, J. Collette, D. Mandry, M. Claudon, O. Pietquin, Functional semi-automated segmentation of renal DCE-MRI sequences, in: *IEEE International Conference on Acoustics, Speech and Signal Processing (ICASSP)*, 2008, pp. 525–528.
- [19] M. S. Aslan, H. A. Munim, A. A. Farag, M. A. El-Ghar, *Biomedical Image Analysis and Machine Learning Technologies: Applications and Techniques*, IGI Global, 2010, Ch. Assessment of Kidney Function Using Dynamic Contrast Enhanced MRI Techniques, pp. 214–233.
- [20] L. Dalla-Palma, G. Panzetta, R. Pozzi-Mucelli, G. Galli, M. Cova, S. Meduri, Dynamic magnetic resonance imaging in the assessment of chronic medical nephropathies with impaired renal function, *Eur Radiol* 10(2) (2000) 280–286.
- [21] N. Michoux, J.-P. Vallee, A. Pechere-Bertschi, X. Montet, L. Buehler, B. Van Beers, Analysis of contrast-enhanced MR images to assess renal function, *Magnetic Resonance Materials in Physics, Biology and Medicine* 19 (2006) 167–179.
- [22] Y. Sun, J. Moura, C. Ho, Subpixel registration in renal perfusion MR image sequence, in: *Proc. 2004 IEEE Int. Symp. Biomed- ical Imaging*, 2004, pp. 700–703.
- [23] A. Agildere, N. Tarhan, G. Bozdagi, A. Demirag, E. Niron, M. Haberal, Correlation of quantitative dynamic magnetic resonance imaging findings with pathology results in renal transplants: A preliminary report, *Transplantation Proceedings* 31(8) (1999) 3312–3316.
- [24] D. Mahapatra, Y. Sun, Rigid registration of renal perfusion images using a neurobiology-based visual saliency model, *Eurasip Journal of Image and Video Proc.* (2010) 4:1–4:22.
- [25] D. Mahapatra, Y. Sun, Registration of dynamic renal MR images using neurobiological model of saliency, in: *5th IEEE International Symposium on Biomedical Imaging: From Nano to Macro (ISBI)*, 2008, pp. 1119–1122.
- [26] Y. Boykov, V. Lee, H. Rusinek, R. Bansal, Segmentation of dynamic N-D data sets via graph cuts using Markov models, in: *Proceedings of the 4th Int. Conf. on Medical Image Computing and Computer-Assisted Intervention (MICCAI)*, 2001, pp. 1058–1066.
- [27] T. Song, V. S. Lee, Q. Chen, H. Rusinek, A. F. Laine, An auto- mated three-dimensional plus time registration framework for dynamic mr renography, *Journal of Visual Communication and Image Representation* 21 (1) (2010) 1–8.
- [28] G. Gerig, R. Kikinis, W. Kuoni, G. van Schulthess, O. Kubler, Semiautomated ROI analysis in dynamic MRI studies: Part I: image analysis tools for automatic correction of organ dis- placements, *IEEE Trans. Image Proc.* 11:(2) (1992) 221–232.
- [29] E. Giele, J. de Priester, J. Blom, J. den Boer, J. van Engelshoven, A. Hasman, M. Geerlings, Movement correction of the kidney in dynamic MRI scans using FFT phase difference movement detection, *J. Magn Reson Imaging* 14(6) (2001) 741–749.
- [30] J. dePriester, A. Kessels, E. Giele, J. denBoer, M. Christiaans, A. Hasman, J. van Engelshoven, MR renography by semiautomated image analysis: performance in renal transplant recipients, *J. Magn Reson Imaging* 14(2) (2001) 134–140.
- [31] F. Khalifa, G. M. Beache, G. Gimel'farb, J. S. Suri, A. S. El-Baz, *Multi modality state-of-the-art medical image segmentation and registration methodologies*, Springer New York, 2011, Ch. State-of-the-Art Medical Image Registration Methodologies: A Survey, pp. 235–280.
- [32] A. El-Baz, G. Gimel'farb, M. A. El-Ghar, New motion correction models for automatic identification of renal transplant rejection, in: *Proceedings of the 10th international conference on Medical image computing and computer-assisted intervention (MICCAI)*, 2007, pp. 235–243.
- [33] R. Sance, M. J. L. Carbayo, A. Lundervold, A. Santos, Image registration for quantitative analysis of kidney function using MRI, in: *5th International Workshop on Information Optics (WIO)*, Vol. 860, 2006, pp. 420–426.
- [34] R. Sance, M. Ledesma-Carbayo, A. Lundervold, A. Santos, Alignment of 3D DCE-MRI abdominal series for optimal quantification of kidney function, in: *5th Int. Symp. on Image and Signal Proc. and Analysis*, 2007, pp. 413–417.
- [35] Y. Sun, M. Jolly, J. M. F. Moura, Integrated registration of dynamic renal perfusion MR images, in: *Proc. 2004 IEEE Int. Conf. on Image Proc.*, 2004, pp. 1923–1926.
- [36] T. Song, V. Lee, H. Rusinek, S. Wong, A. Laine, Integrated four dimensional registration and segmentation of dynamic renal MR images, in: *Medical Image Computing and Computer-Assisted Intervention (MICCAI)*, Vol. 4191,

2006, pp. 758–765.

- [37] P. Yim, H. Marcos, M. McAuliffe, D. McGarry, I. Heaton, P. Choyke, Registration of time-series contrast enhanced magnetic resonance images for renography, in: Proc. 14th IEEE Symp. Computer Based Medical Systems, 2001, pp. 516–520.
- [38] K. Passera, L. Mainardi, D. McGrath, J. Naish, D. Buckley, S. Cheung, Y. Watson, A. Counce, G. Buonaccorsi, J. Logue, M. Taylor, C. Taylor, J. Waterton, H. Young, G. Parker, A non-linear registration method for DCE-MRI and DCE-CT comparison in bladder tumors, in: IEEE Int. Symp. on Biomedical Imaging: From Nano to Macro, 2008, pp. 1095–1098.
- [39] D. Zikic, S. Sourbron, X. Feng, H. J. Michaely, A. Khamene, N. Navab, Automatic alignment of renal DCE-MRI image series for improvement of quantitative tracer kinetic studies, in: SPIE Medical Imaging, San Diego, California, USA, 2008.
- [40] A. D. Merrem, A variational approach to image registration in DCE-MRI of human kidney, in: Proc. Intl. Soc. Mag. Reson. Med., Vol. 19, 2011, p. 815.
- [41] K. E. Jannin P, W. S., Guest editorial validation in medical image processing, Medical Imaging, IEEE Transactions on 25 (11) (2006) 1405–1409.
- [42] J. Pluim, J. Maintz, M. Viergever, Mutual information based registration of medical images: A survey, IEEE Trans on Medical Imaging 22 (8) (2003) 986–1004.
- [43] A. Collignon, F. Maes, D. Delaere, D. Vandermeulen, P. Suetens, G. Marchal, Automated multimodality image registration using information theory, in: Proceedings of Information Processing in Medical Images, 1995, pp. 263–274.
- [44] P. Viola, W. Wells, Alignment by maximization of mutual information, in: Proc. 5th Int. Conf. Computer Vision, 1995, pp. 16–23.
- [45] F. Maes, D. Vandermeulen, P. Suetens, Comparative evaluation of multiresolution optimization strategies for multimodality image registration by maximization of mutual information, Medical Image Analysis 3 (1999) 373–386.
- [46] F. Maes, A. Collignon, D. Vandermeulen, G. Marchal, P. Suetens, Multimodality image registration by maximization of mutual information, IEEE transactions on Medical Imaging 16 (2) (1997) 187–198.
- [47] C. Studholme, D. L. G. Hill, D. J. Hawkes, An overlap invariant entropy measure of 3D medical image alignment, Pattern Recognition 32 (1) (1999) 71–86.
- [48] L. Ibanez, W. Schroeder, L. Ng, J. C. et al., The ITK Software Guide, Kitware, Inc., 2005. URL <http://www.itk.org/>
- [49] L. Devroye, Non-Uniform Random Variate Generation, Springer-Verlag New York, 1986.